JOURNAL OF APPLIED ELECTROCHEMISTRY 15 (1985) 591–601

*Determination of state-of-discharge of zinc–silver oxide button cells. III. In situ impedance measurements of each electrode**

JEAN-PAUL RANDIN

ASULAB S.A., Passage Max-Meuron 6, 2001 Neuchâtel, Switzerland

Received 1 June 1984; revised 10 July 1984

The ac impedance of each electrode of Zn–Ag_2O button cells (30–50 mA h) has been measured over an extended range of frequencies using a Hg/HgO reference electrode located in a small hole drilled through the positive case terminal. The high frequency impedance spectrum of the Ag_2O cathode is a straight line with a 22.5° slope typical for diffusion at a porous electrode. The low frequency end exhibits a 45° sloped straight line characteristic of diffusion processes at a planar electrode. The deposition process is fast and hence the change transfer resistance is usually not clearly evident in the complex plane impedance plot. The impedance response of the zinc anode shows a capacitive loop at high frequencies and some inductive effects characteristic of adsorption processes. At low frequency the complex plane impedance plot of the total cell is a straight line of slope close to 45° mainly ascribed to the Ag_2O cathode. At high frequencies equally important contributions from the two electrodes are evident. The main change in impedance which results from discharge is the decrease of the characteristic relaxation frequency of the high frequency capacitive loop of the zinc anode. The determination of the state-of-discharge at a frequency higher than 1 Hz is best realized if (i) the characteristic relaxation frequency of the high frequency capacitive loop occurring at the zinc anode decreases with discharge and (ii) the response of the Ag_2O cathode is quasi-linear over the entire frequency range. Under these conditions the characteristic relaxation frequency at the zinc anode or some related parameters can be clearly seen on the spectrum measured at the two terminals and used as a state-of-discharge indicator.

1. Introduction

The impedance of primary cells incorporating a zinc anode has recently been studied extensively [1–9]. The Leclanché [1–3], the alkaline zinc–manganese dioxide [4–7], and the alkaline zinc–mercuric oxide cells [8] were studied but no data are available for the alkaline zinc–silver oxide (monovalent) cell which is widely used to power watches, pocket calculators, cameras, hearing aids and other consumer products.

The main aim of the present study was to investigate the ac impedance of Zn–Ag_2O cells as the basis for the development of a fast, reliable, nondestructive state-of-discharge indicator. It was known from the data presented in another paper that the impedance response changed markedly on discharge [10]. Some of the changes can be used as a state-of-discharge indicator. Before the changes in frequency response could be ascribed to any particular element, it was necessary to know the impedance characteristics of each electrode. This was achieved by examining the behaviour of each electrode in the same cell using a reference electrode to separate the different contributions. In the present paper it will be shown that the complex plane impedance plot of the zinc anode contains capacitive and inductive loops characteristic of adsorption processes while the response of the silver oxide cathode is mainly determined by diffusion in solution. The low frequency impedance spectrum of the total cell is mainly composed of the solution diffusion Warburg process occurring at the Ag_2O cathode while the high frequency response involves equally important contributions from the two electrodes.

* This is the final part of a series of papers dedicated to Professor Ernest Yeager on the occasion of his 60th birthday.

0021-891X/85 $03.00 + .12

2. Experimental details

Some of the types of low drain cells previously investigated [10] were used. They were mainly the 9.5 x 2.1 mm, 9.5 x 2.6mm and 11.6 x 2.1mm sizes from four different manufacturers. The construction of the button cells has been described recently [11]. The anode, separator and cathode are parallel planes perpendicular to the axis of symmetry of the cell. The size of the cells of interest makes the task of using a reference electrode rather difficult. It was not feasible to study either electrode separately by machining the wall of the positive case because of the physical instability of the electrodes, particularly the powdered zinc anode. A hole drilled through the anode top lid destroyed the integrity of the zinc electrode. The most reliable way to make access to the inside of the cell was to carefully drill a hole (1.7 mm diameter) through the positive case making sure that no short-circuit was established with the opposite electrode during the mechanical operations. The depth of the hole was controlled to avoid damage to the separators. Towards the end of discharge most of the Ag_2O is reduced to metallic silver which forms a hard crust at the cathode surface. The rupture of the latter without disturbing the separator layer was achieved with proper precautions.

A Hg/HgO, 1N NaOH reference electrode (Ingold AG, Urdorf, Switzerland) extended with a stretched polyethylene tube on a 1 mm diameter frit was positioned inside the hole. When necessary, a drop of electrolyte was added to assure good ionic contact to the reference electrode. The measurements were usually carried out in the following order: 1. at the two terminals before drilling the hole; 2. at the two terminals after introducing the reference electrode to check that the response was not significantly different from the first one; 3. at the Ag_2O cathode with respect to the Hg/HgO reference electrode using the zinc anode as a counter electrode; and 4. at the zinc anode with respect to the Hg/HgO reference electrode using the Ag_2O cathode as a counter electrode.

The value of the purely ohmic resistances in the three measurements on a given cell were mainly determined by the relative position of the reference electrode with respect to the cathode and anode and by the addition of a small amount of fresh electrolyte to improve the ionic contact. The high-frequency intercept with the real axis of the impedance plot for each electrode with respect to the reference should therefore not be considered as a significant characteristic of the cell investigated.

After the opening of a cell, measurements were performed as rapidly as possible, usually within 24 h. Such a long time of investigation was required for measurements carried out down to frequencies in the mHz range. After about one day the electrical characteristics of the cell began to drift due to changes of the electrolyte concentration, carbonation, etc. Therefore, it was not possible to measure the same cell at significantly different states-of-discharge. For such an investigation, different cells from the same lot were used. As a significant dispersion was usually observed from one cell to the other only the overall trends of the measurements will be reported in the present paper.

The experimental technique by which the impedance of the cell on open-circuit conditions or under dc current drain was measured at various states-of-discharge, has been described [10].

3. Results

Typical impedance plots of an undischarged cell are shown in Fig. 1a using three different experimental configurations: i. the usual two terminals configuration; ii. the Ag_2O cathode with respect to the Hg/HgO reference electrode; iii. the Zn anode with respect to the Hg/HgO. It has been verified that within the experimental errors, the total cell impedance in the complex plane is equal to the sum of the two partial contributions.

The impedance plot of the Zn anode exhibits a high frequency capacitive loop, an inductive loop and an additional capacitive loop at the lowest frequencies. The capacitive loop may be considered as due to the charge transfer resistance θ in parallel with the double layer capacity. The charge transfer resistance is about 1 $\Omega\,cm^2$ (apparent surface area) which corresponds to an exchange current density of 13 mA (apparent $cm)^{-2}$. The effective surface area of the anode may be determined from the value of the passi-

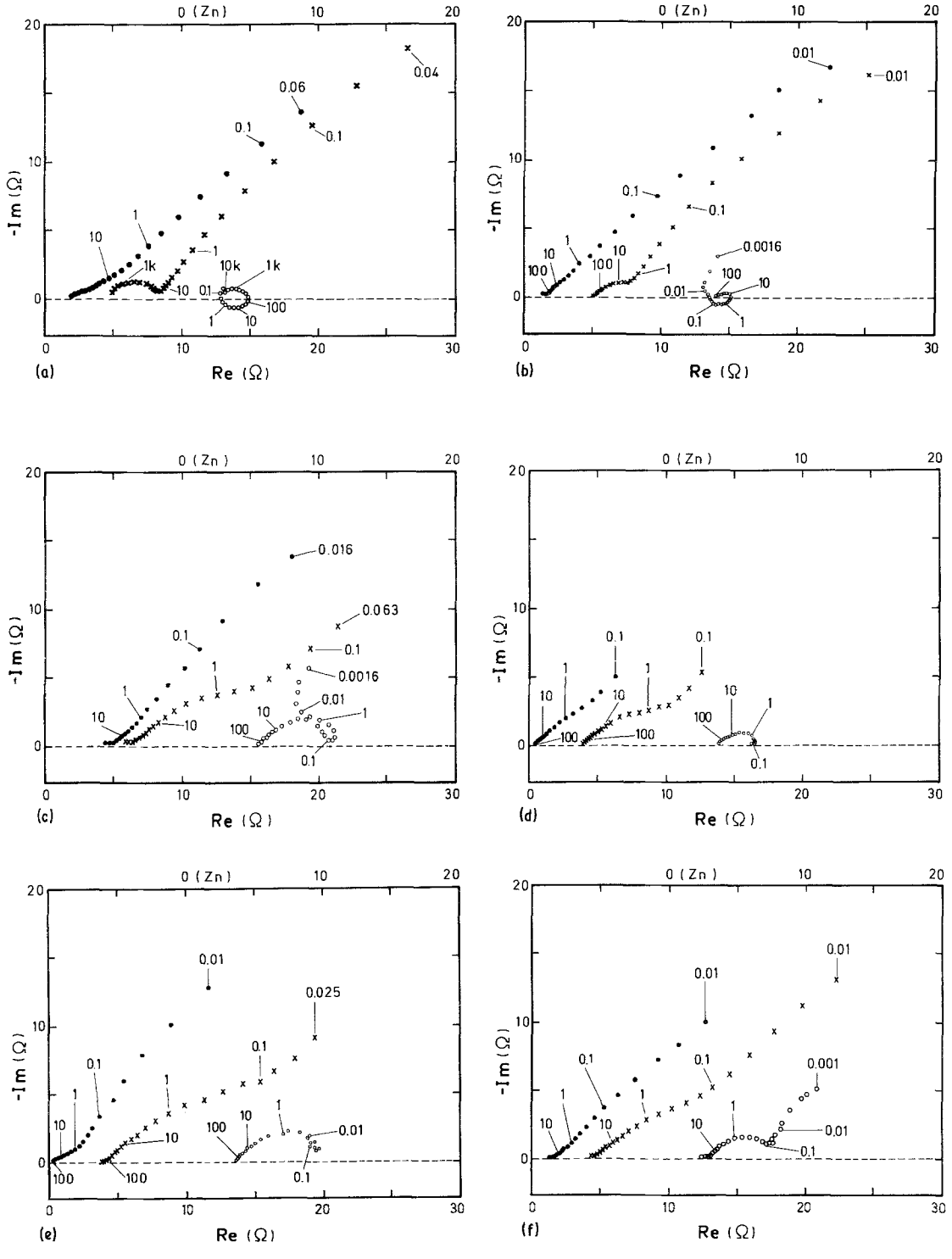

Fig. 1. Complex plane impedance plot of a 11.6 mm × 2.1 mm (manufacturer A) low drain cell using three measurement configurations: i. the normal two terminal measurement (×); ii. the Ag_2O cathode relative to the Hg/HgO reference electrode (•), and iii. the Zn anode relative to the Hg/HgO (○). In (a) the undischarged state, (b) at 20, (c) 40, (d) 60, (e) 80 and (f) 90% state-of-discharge. Note the shift of zero used for the Zn anode (upper scale). Number adjacent to points refers to frequency in Hz.

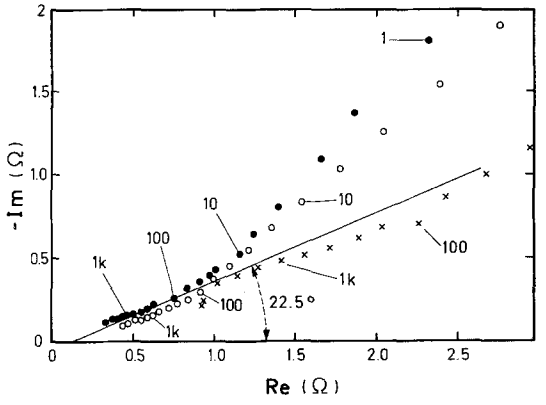

Fig. 2. High frequency complex plane impedance plots of the Ag_2O cathode for the data corresponding to Fig. 1a, undischarged cell (×); Fig. 1b, 20% state-of-discharge (○) and Fig. 1d, 60% state-of-discharge (●). The curves have been shifted along the real axis for an easy comparison.

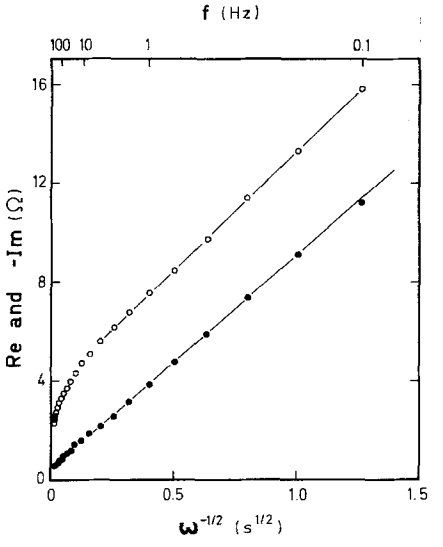

Fig. 3. Randles plot of the impedance data corresponding to Fig. 1a; Re (○), — Im (●).

vation time [12]. A value of $i\tau^{1/2} = 58\,\text{mA s}^{1/2}$ corresponding to an effective surface area of $0.30\,\text{cm}^2$ was found. The latter value is smaller than the apparent surface area ($0.48\,\text{cm}^2$) due to the exceptionally low value of the passivation time found for this particular lot number. Thus the exchange current density per effective area is found to be about 21 mA (eff. cm)$^{-2}$. The double layer capacity is found to be between 110 and 180 μF cm^{-2}. The inductive loop shown in Fig. 1a indicates only one time constant. Such a loop is characteristic of reactions involving adsorbed intermediates.

The impedance plot of the Ag_2O cathode shown in Fig. 1a consists of two straight lines with a slope of about 22° at high frequencies (see Fig. 2) and 45° at low frequencies (see Fig. 1a). Porous electrode behaviour is observed at high frequencies while equivalent planar behaviour is seen at lower frequencies as the ac field penetrates the pore networks. The critical frequency when the behaviour reverts from porous to planar or vice versa is between 10 and 100 Hz. The low frequency line is typical of a solution diffusion Warburg impedance. A Randles representation (R and $1/\omega C$ vs $\omega^{-1/2}$) is shown in Fig. 3 for the low-frequency data of an undischarged cell.

The total cell impedance consists of a low frequency quasi-straight line of slope between 40 and 50° mainly due to the Ag_2O cathode and a high-frequency loop in which an equally important contribution from each electrode is evident (see Fig. 1a).

The impedance diagram for typical undischarged cells from three different manufacturers are shown in Figs. 4–6. Some differences are evident from one type to the other but the main

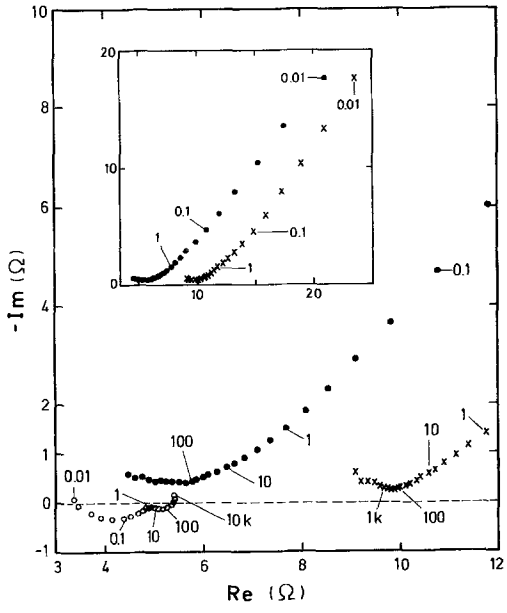

Fig. 4. Impedance plot of an undischarged 11.6 mm × 2.1 mm (manufacturer B) low drain cell measured at the two terminals (×), and at the Ag_2O (●) and Zn (○) electrodes relative to the reference electrode.

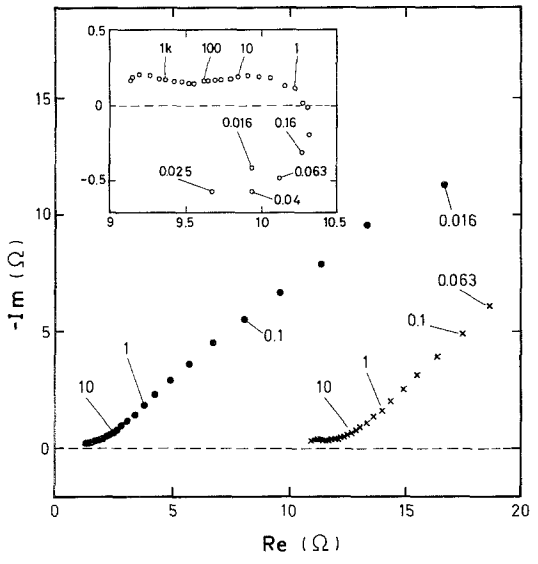

Fig. 5. Same as Fig. 4 for an undischarged 9.5 mm × 2.1 mm (manufacturer C) low drain cell.

general trends remain unchanged. In the case of Fig. 4, the impedance plot of the zinc anode is inductive from 2.5 kHz down to 0.01 Hz with two well-defined relaxation frequencies at 25 and 0.1 Hz. In Fig. 5 the high frequency capacitive loop of the zinc anode is elongated and may be considered as the envelope of a series of semi-circles centred on the real axis. The high-frequency end of the Ag_2O cathode is a straight line of slope close to 22° in Fig. 5, while in Fig. 6 a semi-circle is clearly evident. From the latter an apparent charge transfer resistance of about 0.5 Ω cm^2 and an apparent double layer capacity of 50 μF cm^{-2} can be calculated. By contrast, the low frequency straight line exhibits roughly the same 45° slope for all the types of cell investigated.

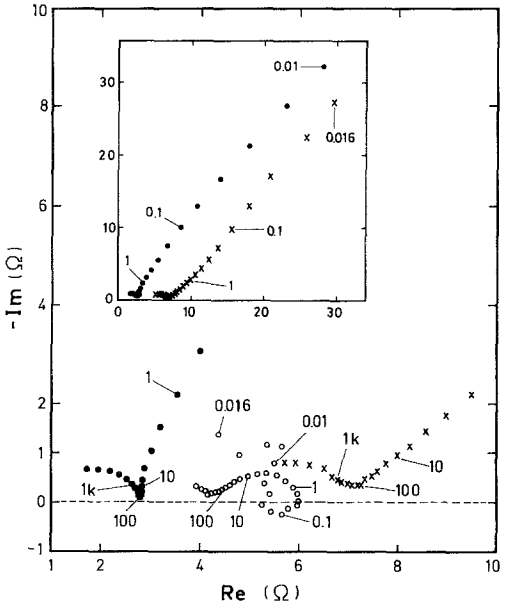

Fig. 6. Same as Fig. 5 for manufacturer E.

The typical changes in impedance which result from discharging are shown in Figs. 1b–f. It should be pointed out that the data shown in Figs. 1a–f are typical of the type of cell investigated and that some variations were observed from one type of cell to the other and also from one manufacturer to the other. At the zinc anode the characteristic relaxation frequency of the high frequency capacitive loop decreased from about 1500 Hz in the undischarged state (Fig. 1a) to about 25 Hz at 20% state-of-discharge (Fig. 1b) and then remained roughly stable in the vicinity of 1 Hz from 40 to 100% state-of-discharge (Figs. 1c–f). The calculated capacity was in the mF cm^{-2} range or higher, indicating that it cannot be attributed to the double layer only but contained some faradaic contribution (Table 1). It is worth noting that the inductive loop disappeared above 40% state-of-discharge.

The general shape of the ac impedance plot of the silver oxide cathode did not change significantly with discharge. The module of the impedance at a given low frequency decreased with discharge resulting in a 2–3-fold decrease of the slope of the Randles plot from the undischarged to the nearly exhausted cell.

The effect of current drain on the impedance response of undischarged cells is shown in Figs. 7 and 8 for each electrode with respect to the

Table 1. Charge transfer resistance and double-layer capacity at the zinc anode calculated from the high frequency semi-circle corresponding to Fig. 1

State-of-discharge	θ (Ω)	C_{dl} (μF)
0	2.0	50
20	0.9	7 100
40	6.7	15 000
60	2.0	32 000
80	5.0	51 000
90	4.2	63 000

reference. The total cell impedance of the same type of cell has been reported elsewhere [10]. At the zinc anode the dc current level influenced mainly:

i. the shape of the inductive loop at low frequency which exhibited an intermediate less inductive loop at the lowest frequencies,

ii. the characteristic relaxation frequency of the capacitive loop which increased from 1 to 4 kHz when the current increased from 0 to 1.5 mA, and

iii. the value θ which decreased with increasing current level. Quantitatively, these changes were relatively small compared to variations occurring at the Ag_2O cathode (Fig. 8). The complex plane plot of the silver oxide electrode indicated that the locus returned to the real axis at low frequencies. The larger the current level, the sharper the bending to the real axis.

Thus, the main effect of the dc current level observed on the total cell impedance (see Fig. 14 of Part II [10]) can be attributed to the Ag_2O cathode at low frequencies and to the zinc anode in the high frequency region.

As compared to the undischarged cells, a smaller effect of the dc current level on the Ag_2O cathode and no significant change on the Zn anode were found for partially discharged cells.

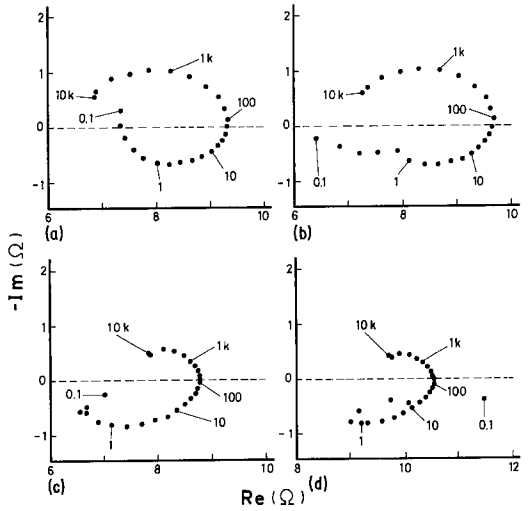

Fig. 7. Effect of the dc current level on the impedance plot of the zinc anode of the same type of cell as in Fig. 1 in the undischarged state. (a) under zero dc current, (b) 0.5, (c) 1.0 and (d) 1.5 mA.

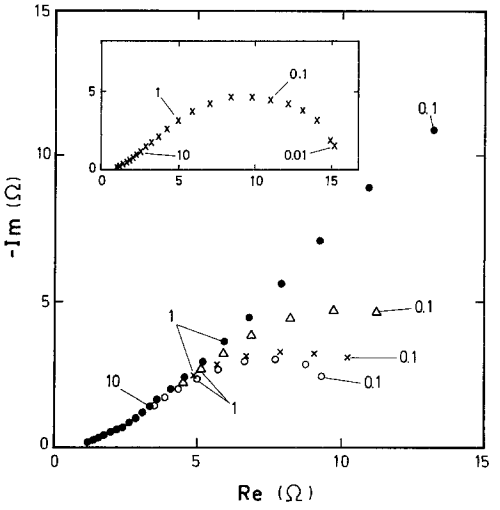

Fig. 8. Same as Fig. 7 for the Ag_2O cathode, (•) under zero dc current, (△) 0.5, (×) 1.0 and (○) 1.5 mA. Insert shows the impedance plot down to 0.01 Hz at 0.75 mA for another sample of the same type of cell.

4. Discussion

4.1. *Zinc anode*

Despite numerous investigations, no definite and generally accepted kinetics and reaction mechanism for the deposition and dissolution of zinc in alkaline solutions have as yet been established. There appears to be a growing consensus that the zinc electrode reaction proceeds in a *cece* mechanism [13–16], where *c* and *e* denote a chemical and electrochemical step, respectively. The rate determining step (rds) is most likely related to the nature of the zinc electrode. At a solid zinc electrode the rds is the first electron transfer step in the cathodic direction [14], whereas it is the chemical step between the two electrochemical steps for a zinc amalgam [15]. A low frequency inductive impedance has been reported which is in agreement with the possible existence of adsorbed intermediates at the electrode surface [17–18]. The faradaic impedance reveals four relaxation processes during either deposition or dissolution in alkaline electrolytes [18].

The general shape of the impedance plot in the undischarged state shown in Fig. 1a is in good agreement with the data published by

Cachet, Ströder and Wiart [18] at an unamalgamated sheet zinc electrode. These authors obtained four relaxation processes while our data show only two or three. This discrepancy may be related to the amalgamation and/or the porosity of the zinc anode as well as to the presence of additives in the electrolyte. The exchange current density calculated from the high frequency capacitive loop is between 13 and 21 mA cm^{-2}, a value in agreement with those reported in the literature for zinc electrodes in 8N KOH + zincate electrolyte at ambient temperature, i.e. 8–370 mA cm^{-2} (see e.g. Bockris, Nagy and Damjanović [14] and Dirkse [16]). The double-layer capacity in parallel with the charge transfer resistance is about 150 μF cm^{-2}.

The decrease of the charge transfer resistance with the increase of the current level shown in Fig. 7 is also in agreement with results reported by Cachet, Ströder and Wiart [18] on planar electrodes. The product of the resistance θ and current remains approximately constant [1.3–1.7 mV] indicating an irreversible and exponentially activated charge transfer [19].

The characteristic relaxation frequency of the high frequency capacitive loop decreased significantly with discharge. The calculated capacity in the partly discharged state is in the mF cm^{-2} range or higher, indicating that it contains some faradaic contribution (see Table 1). The shift of the characteristic relaxation frequency or some related parameters can be used as a state-of-discharge indicator. Such a parameter is very attractive since it is an intensive parameter, i.e. it does not depend on the amount of active material.

The details of the impedance plot of the zinc anode for the undischarged cells may change for each dimension and each manufacturer (see Figs. 1a and 4–6). Variations in the adsorption stages are expected to occur with changes in the nature and concentration of organic additives used in the electrolyte, e.g. sodium carboxymethyl cellulose used as a gelling agent.

In summary, the general aspect of the impedance plot of the zinc anode is in agreement with the published data for a planar electrode. The porous nature of the zinc anode is not clearly evident from the impedance plots, and this irrespective of the state-of-discharge. Karunathilaka *et al.* [5] observed a similar behaviour for the alkaline Zn–MnO_2 cell measured at the two terminals and explained it by the fact that a quasi-planar reaction zone may occur at the front electrode and progress into the porous mass as the reaction proceeds. The product of the process is ZnO which remains as a porous structure overlaying the unreacted zinc. The electrolyte–electrode interface may therefore by considered as a 'porous electrolyte' and a quasi-planar electrode rather than a porous electrode reacting in depth.

4.2. *Silver oxide cathode*

The proposed reaction path involves a dissolution–precipitation mechanism in which there is dissolution of silver oxide

$$Ag_2O + 2\ OH^- + H_2O \rightleftharpoons 2\ Ag(OH)_2^- \qquad (1)$$

followed by migration of the dissolved species to an electronically conducting point in the positive mass where it is reduced to metallic silver

$$Ag(OH)_2^- + e \rightarrow Ag + 2\ OH^- \qquad (2)$$

The high frequency part of the impedance plots of the Ag_2O cathode (Fig. 2) shows a typical solution diffusion Warburg behaviour for a porous electrode with semi-infinite pores since the slope is close to 22.5°. The behaviour changes from porous to planar at a critical frequency between 10 and 100 Hz. The low frequency line exhibits a slope of about 45°. For a purely solution diffusion process the critical frequency ω'^* is related to the pore length l and pore radius r by the relation [20]

$$\omega'^{*1/2} = \frac{\sigma' r}{(2)^{1/2}\pi\rho l^2} \qquad (3)$$

Here σ' is the Warburg coefficient for diffusion in solution related to an apparent unit area in $\Omega\ cm^2\ s^{-1/2}$ and ρ is the electrolyte resistivity in Ω cm. Using $\sigma' = 4.3\ \Omega\ cm^2\ s^{-1/2}$ (from Fig. 3), a critical frequency of 10–100 Hz and a pore radius of 1–5 μm, a pore length of 10–40 μm is calculated. The pore radius was estimated from a scanning electron micrograph of the undischarged cathode.

In addition to the solution diffusion Warburg

characteristic of a porous electrode, small charge transfer contributions corresponding to a rapid deposition process were sometimes evidenced by the partial skewed semi-circles at the highest frequencies (see Fig. 6).

The slope of the Randles plot is given by the equation

$$\sigma = \frac{RI}{(2)^{1/2}n^2F^2S}\left(\frac{1}{C_O D_O{}^{1/2}} + \frac{1}{C_R D_R{}^{1/2}}\right) \quad (4)$$

where σ is in $\Omega\ s^{-1/2}$, S is the surface area in cm^2, C_O and C_R are the concentrations of the oxidized and reduced species, D_O and D_R are the diffusion coefficients of the oxidized and reduced species and the other symbols have their usual significance. In Reaction 2 the diffusing oxidized species $Ag(OH)_2^-$ is reduced to the metal which deposits on the electrode. The term $1/C_{Ag}D_{Ag}^{1/2}$ in Equation 4 can therefore be neglected and the experimental slope may be used to estimate the effective surface area S, using $C_{Ag(OH)_2^-} = 2.3 \times 10^{-7}$ mol cm^{-3} and $D_{Ag(OH)_2^-} = 3.3 \times 10^{-6}$ $cm^2\ s^{-1}$ as measured by Miller [21] by means of a rotating disc electrode in 8 N NaOH, although the electrolyte in the cell of Fig. 1 was NaOH, most likely containing additives. Thus, the slope of about $9\ \Omega\ s^{-1/2}$ found in the Randles plot of Fig. 3 corresponds to a calculated true surface area, S, of 50 cm^2. The low frequency straight line is related to the fully developed area soaked by the electrolyte. The ratio between the true and apparent area is about 100.

The value of the slope σ has been found to decrease with discharge. This may indicate that the effective surface area increases with state-of-discharge. Intuitively, S is expected to decrease with state-of-discharge since the amount of Ag_2O decreases. However, the latter effect could be overcompensated for by an increase in the surface area with discharge due to internal porosity. Such a porosity could originate from a smaller molar volume of Ag compared to that of Ag_2O.

The return of the complex plane impedance curve to the real axis from an initial straight line of slope 45° under the influence of the dc current has been observed (see Fig. 8). The impedance spectrum obtained for the highest current is characteristic of a diffusion process in a finite length layer. At low frequencies the ac diffusion layer becomes comparable with the Nernst diffusion layer and these interact causing a deviation from the normal Warburg impedance [22, 23]. For an irreversible diffusion-controlled charge transfer process assuming Nerstian conditions, the electrode impedance Z is given by [22–24]

$$Z = \theta + R_d \tanh (j\omega\delta^2/D)^{1/2}/(j\omega\delta^2/D)^{1/2} \quad (5)$$

where θ is the charge transfer resistance, R_d is the diffusional resistance, δ is the thickness of the Nernst diffusion layer, and D is the diffusion coefficient of the mobile species. At low frequencies the diffusional impedance relaxes to the real axis where the value of Z, as the frequency tends towards zero, is defined as

$$(Z)_{\omega \to 0} = \theta + \sigma\delta\left(\frac{2}{D}\right)^{1/2} \quad (6)$$

Assuming D independent of current, it can be seen that as the current increases, R_d decreases, and therefore, δ decreases as well (see Fig. 8). A

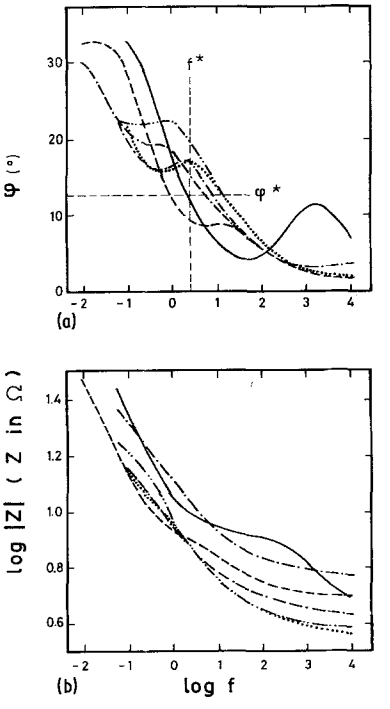

Fig. 9. Bode plots of the total cell impedance corresponding to data in Fig. 1. at 0 (——), 20 (– – –), 40 (–·–·–), 60 (·····), 80 (–·····–·····–) and 90% state-of-discharge.

value of 13 μm is found for δ using $\sigma = 9\ \Omega\ s^{-1/2}$ (see Fig. 3), $R_d = 9\ \Omega$ at $i_{dc} = 1$ mA and $D = 3.3 \times 10^{-6}\ cm^2\ s^{-1}$. The frequency ω^* at the apex of the diffusion loop of the complex plane is given by the expression [24]

$$\omega^* = 2.53\frac{D}{\delta^2} \tag{7}$$

Here again, assuming D to be independent of current, an increase of current corresponds to an increase of ω^* (see Fig. 8) and a decrease of δ. A frequency of 0.8 Hz is found using the δ value calculated above as compared to an experimental value of 0.25 Hz.

The thickness of the Nernst diffusion layer at the limiting current density i_l is given by

$$\delta = \frac{nFDC^*}{i_l} \tag{8}$$

where C^* is the bulk concentration of the mobile species, independent of current density. Assuming a linear dependence of δ with i and D independent of i, an increase of current decreases the Nernst diffusion layer. The data of Fig. 8 are in agreement with this model.

Scanning electron micrographs of the cathode mass have shown significant differences from one manufacturer to the other. Thus, the various high frequency ac impedance responses of the Ag_2O cathode obtained for each manufacturer (Figs. 1 and 4–6) may originate from a different morphology and size of the silver oxide particles.

4.3. *Implications for the state-of-discharge measurements*

The state-of-discharge indicator proposed earlier [10] is based on the measurement of the phase of the impedance or a phase angle corrected for the ohmic resistance at a given frequency. This frequency should be as high as possible to permit a short measurement time. In the example of Fig. 9, a phase angle $\varphi^* < 12.5°$ measured at $f^* = 2.5$ Hz corresponds to a state-of-discharge $\leqq 30\%$. At such a frequency the phase angle is influenced by both electrodes as shown in Figs. 10 and 11. The contribution of each electrode on the phase angle will now be discussed. (It may be recalled that the sum of the phase angle of the

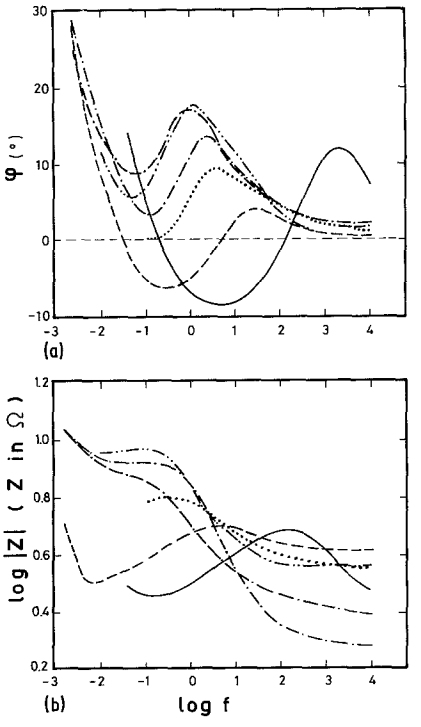

Fig. 10. Bode plots of the total cell impedance corresponding to data in Fig. 1 but for the Zn anode. Data taken at 0 (——), 20 (– – – –), 40 (–·–·–·–), 60 (····), 80 (–···–···–) and 90% state-of-discharge.

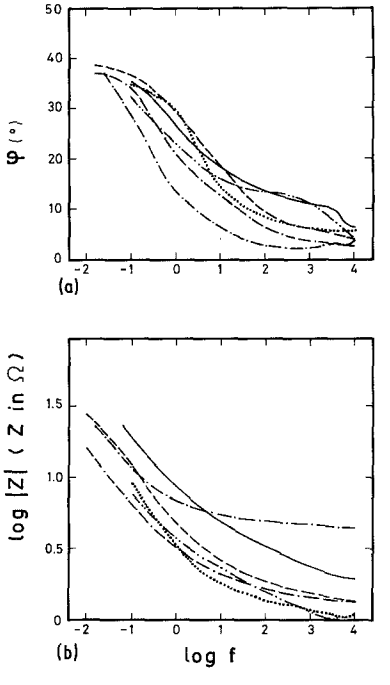

Fig. 11. Same as Fig. 10 for the Ag_2O cathode.

partial contributions at a given frequency is not equal to the phase angle of the total cell impedance.)

The variations of the phase of the impedance of the Ag_2O cathode are too small and scattered to permit a determination of the state-of-discharge (Fig. 11).

At the zinc anode the characteristic relaxation frequency shifts to low frequencies with increasing state-of-discharge (see Fig. 10). This effect is also clearly evident on the measurements performed at the two terminals (see Fig. 9). The characteristic relaxation frequency or the frequency at the minimum between the semi-circle and the straight line occurs at frequencies higher than about 1 Hz. At these frequencies the impedance data are of approximately equal value at each electrode. The significant changes of the phase angle due to the Zn anode can be retrieved from the data measured at the two terminals thanks to the small and regular variations at the Ag_2O cathode. When the complex plane impedance plot of the Ag_2O cathode was curved or contained a semi-circle (Fig. 6) the total cell impedance was too complex to be used for the state-of-discharge determination.

The variation of the absolute value of the phase angle at the characteristic relaxation frequency of the Zn anode shown in Fig. 10 is due to changes of the ohmic resistance from one cell to the other. The corrected phase angle φ' used previously [10] could be used to eliminate this effect.

For most of the types of cells investigated previously the frequency response of the undischarged cell measured at the two terminals was significantly different from that of the partly discharged cells, especially at high frequencies (see Figs. 4–6, 12 and 13 of Part II [10]). For most of the cells this difference was used in the determination of the state-of-discharge. However, for some types of cells, (e.g. Fig. 12 of Part II [10]) it created difficulties in the state-of-discharge determination. The data of Figs. 1 and 9–11, as well as Table 1, show that the change arises from the zinc anode whose frequency response varies significantly between the undischarged and partly discharged states.

For some types of cells the relative variation of each electrode was such that the contribution from the zinc anode at frequencies higher than 1 Hz could not be seen in the measurements performed on the total cell. In that case, most of these cell types could be selected at frequencies lower than 1 Hz, e.g. at 0.16 Hz. However, even at these low frequencies the selection is still made on changes occurring in the zinc anode even though the main contribution to the impedance comes from the Ag_2O cathode. The impedance of the Ag_2O is scattered or decreases slightly with discharge (see Fig. 11). Three different types of behaviour may occur depending on the variations of the impedance of the zinc anode at low frequencies:

1. The impedance of the zinc anode, especially the real component, increases with state-of-discharge (see Figs. 1 and 10) and consequently the phase angle measured at the two terminals decreases (see Fig. 9). This is the most frequently encountered situation.
2. The impedance of the Zn anode decreases and the phase angle of the total cell increases with discharge.
3. The impedance of the Zn anode changes little with state-of-discharge and the variations of the phase angle of the total cell depend on changes occurring at the Ag_2O cathode.

For most of the types investigated the selections performed at a frequency smaller than 1 Hz were based on a φ or φ' value *higher* than the selecting value for state-of-discharge smaller than 20–40%. By contrast, the selection carried out at a frequency higher than 1 Hz correspond to a φ or φ' value *smaller* than the selecting value for a state-of-discharge smaller than 20–40%. This is due to the low value of $\log |Z|$ at low frequencies for the Zn anode at 0 and 20% state-of-discharge as compared to that in the more discharged states (see Fig. 10). Such a low value has a strong effect on the phase angle of the total cell.

Although the main general trends of each electrode are the same for each type of cell and each manufacturer, the details of the changes occurring upon discharge depend significantly on the size and fabrication procedures. The state-of-discharge determination rely on such subtle changes. It is therefore not surprising that a calibration is needed for each type of cell and each manufacturer to determine the optimum parameters for the selection test.

Acknowledgements

The author is pleased to thank F. Züllig for his skillful assistance in the experimental work as well as R. Viennet and R. Wiart (CNRS, Paris) for helpful discussions.

References

[1] S. A. G. R. Karunathilaka, N. A. Hampson, R. Leek and T. J. Sinclair, *J. Appl. Electrochem.* **10** (1980) 357.
[2] *Idem, ibid.* **10** (1980) 603.
[3] *Idem, ibid.* **10** (1980) 799.
[4] M. L. Gopikanth and S. Sathyanarayana, *ibid.* 9 (1979) 581.
[5] S. A. G. R. Karunathilaka, N. A. Hampson, R. Leek and T. J. Sinclair, *ibid.* **11** (1981) 365.
[6] *Idem, ibid.* **11** (1981) 715.
[7] M. Hughes, S. A. G. R. Karunathilaka, N. A. Hampson and T. J. Sinclair, *ibid.* **13** (1983) 217.
[8] S. A. G. R. Karunathilaka, N. A. Hampson, T. P. Haas, R. Leek and T. J. Sinclair, *ibid.* **11** (1981) 573.
[9] S. A. G. R. Karunathilaka, N. A. Hampson, R. Leek and T. J. Sinclair, *J. Power Sources* 9 (1983) 205.
[10] J. P. Randin, *J. Appl. Electrochem.* **15** (1985) 365.
[11] F. L. Tye, in 'Electrochemical Power Sources' (edited by M. Barak) Peter Peregrinus for the IEE, London (1980) pp. 50–150.
[12] J. -P. Randin, *J. Appl. Electrochem.* **15** (1985) 293.
[13] D. A. Payne and A. J. Bard, *J. Electrochem. Soc.* **119** (1972) 1665.
[14] J. O'M. Bockris, Z. Nagy and A. Damjanović, *ibid.* **119** (1972) 285.
[15] A. R. Despic, D. Jovanovic and T. Rakic, *Electrochim. Acta* **21** (1976) 63.
[16] T. P. Dirkse, *J. Electrochem. Soc.* **126** (1979) 541.
[17] R. D. Armstrong and M. F. Bell, *J. Electroanal. Chem.* **55** (1974) 201.
[18] C. Cachet, U. Ströder and R. Wiart, *Electrochim. Acta* 7 (1982) 903 and references therein.
[19] I. Epelboin and M. Keddam, *J. Electrochem. Soc.* **117** (1970) 1052.
[20] R. D. Armstrong, K. Edmondson and J. A. Lee, *J. Electroanal. Chem.* **63** (1975) 287.
[21] B. Miller, *J. Electrochem. Soc.* **117** (1970) 491.
[22] M. Sluyters-Rehbach and J. H. Sluyters, in 'Electroanalytical Chemistry', Vol. 4 (edited by A. J. Bard) M. Dekker, Inc., New York (1970) pp. 1–128.
[23] R. D. Armstrong, M. F. Bell and A. A. Metcalfe, in 'Electrochemistry, Specialist Periodical Report, Vol. 6 (edited by H. R. Thirsk) The Chemical Society, Burlington House, London (1978) pp. 98–127.
[24] J. Bressan, G. Feuillade and R. Wiart, *J. Electrochem. Soc.* **129** (1982) 2649.
[25] T. D. Dirkse, D. DeWit and R. Shoemaker, *ibid.* **114** (1967) 1196.